Genomic adaptations for arboreal locomotion in Asian flying treefrogs

Wei Wu[a,b,1] , Yue-Dong Gao[c,1] , De-Chun Jiang[a,1], Juan Lei[d] , Jin-Long Ren[a,b], Wen-Bo Liao[e], Cao Deng[f] , Zeng Wang[a,b], David M. Hillis[g,2], Ya-Ping Zhang[c,h,2], and Jia-Tang Li[a,b,h,i,2]

[a]Chinese Academy of Sciences Key Laboratory of Mountain Ecological Restoration and Bioresource Utilization & Ecological Restoration and Biodiversity Conservation Key Laboratory of Sichuan Province, Chengdu Institute of Biology, Chinese Academy of Sciences, Chengdu 610041, China; [b]University of Chinese Academy of Sciences, Beijing 100049, China; [c]State Key Laboratory of Genetic Resources and Evolution, Kunming Institute of Zoology, Chinese Academy of Sciences, Kunming 650223, China; [d]Ministry of Education Key Laboratory for Biodiversity Sciences and Ecological Engineering, College of Life Sciences, Beijing Normal University, Beijing 100875, China; [e]Key Laboratory of Southwest China Wildlife Resources Conservation (Ministry of Education), China West Normal University, Nanchong 637009, China; [f]Department of Bioinformatics, DNA Stories Bioinformatics Center, Chengdu 610041, China; [g]Department of Integrative Biology and Biodiversity Center, University of Texas at Austin, Austin, TX 78712; [h]Center for Excellence in Animal Evolution and Genetics, Chinese Academy of Sciences, Kunming 650223, China; and [i]Southeast Asia Biodiversity Research Institute, Chinese Academy of Sciences, Nay Pyi Taw 05282, Myanmar

Adaptations can endow species with complex traits that enable them to occupy new niches. To adapt to the arboreal lifestyle, treefrogs have evolved a suite of complex traits for climbing and gliding; to date, however, the molecular mechanisms underpinning these adaptations are unknown. Here, based on two de novo–assembled Asian treefrog genomes, genes related to limb development showed evidence of accelerated evolution. Furthermore, the *PPL* gene that regulates the keratin cytoskeleton showed conservative substitution within the genus *Rhacophorus*. These genetic changes contribute to limb and toe-pad morphogenesis, providing fundamental adaptations for climbing and grasping. Behavioral and morphological comparisons clarified the gliding function of interdigital webbing and the different developmental patterns between fully and weakly webbed feet. Time-ordered gene coexpression network analysis of gliding *Rhacophorus kio* and nongliding *Rhacophorus dugritei* tadpoles revealed specific coexpression patterns for fully webbed feet, which involved the Wnt signaling and vascular remodeling pathways. These findings highlight the molecular basis of phenotypes that facilitate expansion into new niches and provide insights into the importance of local adaptation in shaping phenotypes and locomotion patterns.

arboreal adaptation | locomotion patterns | complex traits | gene coexpression | treefrogs

Arboreal species provide an excellent opportunity for investigating adaptations to new ecological niches. Expansion into an arboreal niche can help improve ground-dwelling predator avoidance as well as access to new food resources and shelter; however, arboreal habitats also create challenges regarding vertebrate locomotion (1, 2). Arboreal animals that reside in tree and forest habitats must cope with travel on unstable and vertical substrates, overcome the risk of falling, and develop ways to cross gaps. These activities are energetically costly and often risky (3). Consequently, limb morphological adaptations are expected to provide species with opportunities to expand into new niches (1, 4, 5).

After the mass extinction event at the end of the Cretaceous, three major anuran families (Rhacophoridae, Hylidae, and Phyllomedusidae)—which diverged ~42.5 Ma, ~49.5 Ma, and ~24.5 Ma, respectively—evolved climbing and/or gliding adaptations independently (6). The evolution of climbing ability, as a prerequisite for the arboreal lifestyle, especially for nonflying species, is a critical adaptation to reduce the risk of falling (7). Climbing in arboreal frogs involves sophisticated skeletal and adhesive toe-pad systems. Notably, arboreal frogs possess longer and more flexible forelimbs and hands than nonarboreal species to facilitate gripping and grasping (4, 5, 8). In addition, species in Rhacophoridae have a bony knob on the third

metacarpal, which enhances gripping (5), as well as Y-shaped intercalary elements within the terminal phalanges, which support well-developed adhesive toe pads. These flattened and enlarged toe pads provide adhesion to wet and slippery surfaces (7, 9). Unlike van der Waals force used by geckos (10), this adhesion system uses capillary force and friction (9). Little structural variation in these adhesive pads is found among independently evolved arboreal frogs, indicating convergence across groups (11). These unique skeletal morphologies and adhesive toe pads appear to be adaptations to the arboreal lifestyle.

Gliding can help frogs traverse the gaps between trees but requires the ability to perform controlled landings (12). Flying frogs usually inhabit the tree canopy. For instance, *Rhacophorus kio* (known as flying frogs) are known to inhabit dipterocarp trees (~62 m tall) at heights of 34.6 m to 57.0 m (13). Flying frogs share a variety of morphological characteristics to facilitate gliding behavior and aerodynamic stability, including enlarged, extensive interdigital webbing and lateral skin flaps on their elbows and ankles (14). As lateral skin flaps occupy a smaller area than full interdigital webbing, webbing may be a

EVOLUTION

more essential adaptation for gliding (14). Notably, weakly webbed treefrogs (e.g., *Rhacophorus dugritei*) that occupy shrub and swamp habitats do not have the ability to glide. In addition, grasping the surface of a substrate is also important for animals to avoid falling from heights. In flying frogs, the manus and pedal webbing, together with adhesive toe pads and modifications of forelimbs, provide effective grasping force to reduce the risks of falling.

Members of the genus *Rhacophorus* provide a unique case for studying the genetic basis of traits that are causally linked to vertical niche expansion. Here, we assembled two Asian treefrog genomes de novo, i.e., those of gliding *R. kio* and nongliding *R. dugritei*, and conducted morphological and behavioral experiments to identify phenotypic similarities and differences in locomotion. Furthermore, we performed comparative genomic and transcriptomic analyses to determine the genetic basis of the unique traits that may assist in climbing and gliding, and thereby facilitate niche expansion. We expect these data to supply a useful genetic resource for future research, especially in the study of adaptive evolution of amphibians.

Results and Discussion

Morphological and Behavioral Differences between *R. kio* and *R. dugritei*. Both species possess terminal phalanges, bony metacarpal knobs, a prepollex, and toe pads, but the extent of manus and pedal webbing differs considerably between the two species (Fig. 1 *A* and *B* and *SI Appendix*, Table S1). When falling from heights of 1, 1.5, and 2 m, the horizontal angle of descent was smaller for *R. kio* than for *R. dugritei* (Fig. 1 *C–F* and *SI Appendix*, Table S2). Unlike *R. dugritei*, *R. kio* stretched

out their hands and feet when falling (Movie S1). These observations point to the fundamental role of interdigital webbing in successful gliding, as observed in *R. kio*.

Some arboreal *Rhacophorus* species can glide due to their relatively extensive manus and pedal webbing (e.g., *Rhacophorus annamensis*, *Rhacophorus hoanglienensis*, *R. kio*, *Rhacophorus reinwardtii*, *Rhacophorus pardalis*, and *Rhacophorus nigropalmatus*), whereas swamp-inhabiting species with weakly webbed hands or feet, such as *R. dugritei*, do not exhibit such behavior (data from https://amphibiaweb.org/). This suggests that webbing confers an advantage and may provide opportunities to expand into higher vertical niches, as gliding is an effective measure to reduce the risk of falling. Further, the gliding ability might facilitate arboreal animals' avoiding predators and increasing their locomotor or foraging efficiency (2). However, webbing is not the only driver of gliding, with body size, lateral skin flap development, and behavior all playing a role in this adaptation. For instance, *Rhacophorus smaragdinus* have fully webbed hands and feet but cannot glide due to their large body size. In addition, a certain degree of climbing behavior is shared by all arboreal frogs and is not the only adaptation leading to vertical niche differentiation, but it is a prerequisite for invading arboreal niches, especially for nonflying species (7).

Genomic Characteristics and Chromosomal Evolution. We assembled two treefrog genomes de novo, i.e., the gliding *R. kio* and nongliding *R. dugritei*. Sequence fragments (143.47 Gb, ~54× coverage) of PacBio long reads from a female *R. kio* (Fig. 1*A*) were assembled into contigs. After using Illumina-based paired-end 150-bp short reads to correct sequence errors, we anchored and oriented the resulting contigs into superscaffolds
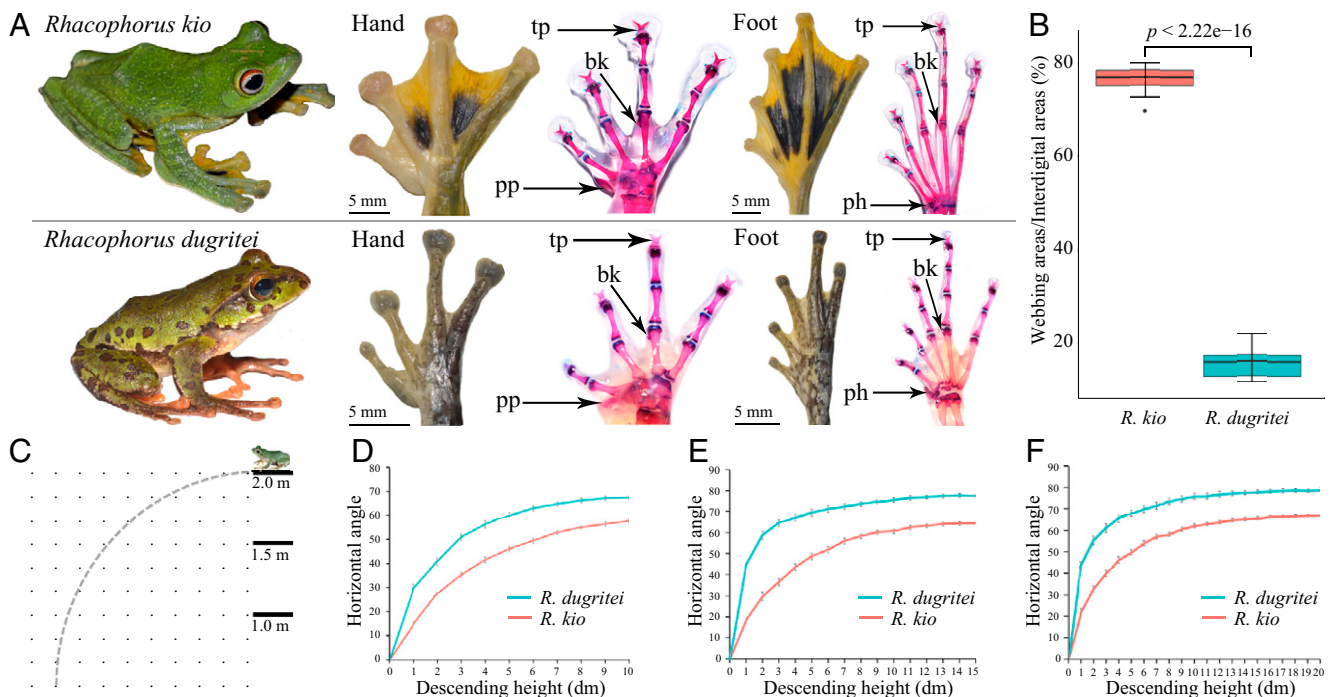

Fig. 1. Morphological comparison and behavioral experiments for *R. kio* and *R. dugritei*. (*A*) Comparison of foot morphology. Both species evolved adhesive toe pads and specialized phalanges, such as prehallux, prepollex, bony knob, and terminal phalanx. Webbed areas in the interdigital regions differ. *R. kio* possesses full webbing, while the feet of *R. dugritei* are weakly webbed. tp: terminal phalanx, pp: prepollex, bk: bony metacarpal knob, ph: prehallux. (*B*) Comparison of interdigital webbing sizes of two typical treefrogs either inhabiting trees (*R. kio*) or swamps (*R. dugritei*). Relative webbed areas of *R. kio* and *R. dugritei* differed significantly. We assessed the relative areas of webbed interdigital tissues of 10 adult males of each species in comparison with their overall interdigital areas. Morphological measurement used a square grid method and significance of differences was calculated by Student's *t* test. (*C*) Schematic of treefrog gliding experiments. (*D*) Descent from ground clearances of 1 m. (*E*) Ground clearances of 1.5 m. (*F*) Ground clearances of 2 m. Ground clearances (centimeters) are along the *x* axis, and horizontal angles are along the *y* axis. Curves in *D*, *E*, and *F* are the line of descent angle, not the gliding trajectory. Horizontal angle of descent in *R. kio* was smaller than that of *R. dugritei* regardless of height. SD is indicated in *D*, *E*, and *F*.

using Hi-C technology. Based on the *Rhacophorus* karyotypes (i.e., 2n = 26) (15), we used Hi-C data to assign the scaffolds to 13 pseudochromosomes, consisting of five macrochromosomes and eight microchromosomes, ranging from 86.9 Mb to 396.5 Mb (Fig. 2*A* and *SI Appendix*, Table S3). Finally, we generated a 2.66-Gb chromosomal-anchored genome for *R. kio* (contig N50 = 1.17 Mb, scaffold N50 = 300.07 Mb; *SI Appendix*, Table S4). The genomic landscape of *R. kio* showed the GC content of different regions of the chromosomes, as well as the distribution patterns of transposable elements (TEs), tandem repeats, and genes (inner to outer rings, respectively, in Fig. 2*B*). In addition, a few chromosomal collinearity blocks were found between or within the chromosomes (Fig. 2*B*). For *R. dugritei*, we assembled the draft genome via a hybrid strategy (see *Materials and Methods* and *SI Appendix, SI Text*), yielding a 3.36-Gb genome (contig N50 = 1.55 Mb; *SI Appendix*, Table S5). We assessed assembly quality using benchmarking of universal

single-copy orthologs (BUSCO v3) (16) and retrieved 83.33% and 87.94% complete BUSCO genes for the *R. kio* and *R. dugritei* genomes, respectively (*SI Appendix*, Fig. S1 and Table S6). To date, eight chromosomal-level anuran genomes from six families (Pipidae, Megophryidae, Pyxicephalidae, Myobatrachidae, Dicroglossidae, and Bufonidae) have been sequenced (*SI Appendix*, Table S6), but none of them inhabit arboreal niches. The chromosomal-level rhacophorid genome in this study will supply important genetic resources and facilitate future studies on adaptive evolution among amphibians.

The *R. kio* and *R. dugritei* genomes contained 46.01% (1.22 Gb) and 38.52% (1.29 Gb) of repetitive sequences (*SI Appendix*, Table S7). In these two treefrogs, one major expansion of repetitive sequences exhibits 0.02 to 0.03 divergence from the consensus sequence (Fig. 2*C*). Further, the TE types and the expansion patterns between *Rhacophorus* and *Xenopus* were quite different (Fig. 2*C* and *SI Appendix*, Table S8).
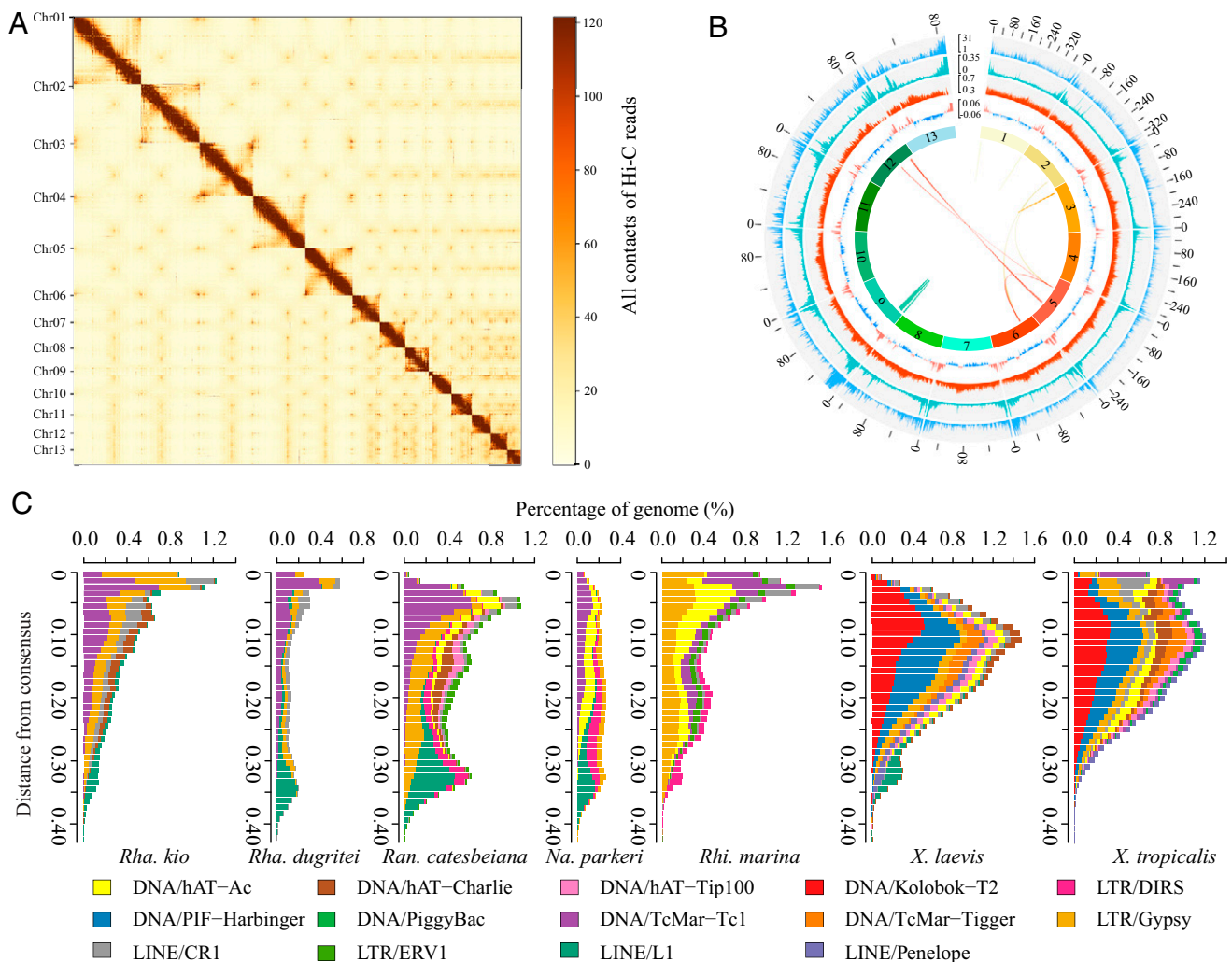
Fig. 2. Genomic landscape of flying frog (*R. kio*) and comparisons of TEs in selected genomes. (*A*) Hi-C interactions among the 13 chromosomes of *R. kio*. Darker color indicates stronger interactions. (*B*) Circos diagram depicting four characteristics of the *R. kio* genome. From inner to outer rings, amount of GC content, TEs, tandem repeats, and genes, respectively. The distribution was computed in overlapping 500-kb windows (with 250-kb step size). The distribution of GC content is equal to the GC content in the window minus the GC content on the corresponding chromosome; the distribution of TEs or tandem repeats is equal to the total length of TEs or tandem repeats in the window divided by the window size; gene density is equal to the number of genes in a window divided by the window size. Arches inside Circos diagram show collinear blocks between or within chromosomes, which are linked by the same-colored lines. (*C*) Comparisons of TEs in selected genomes. *x* axis shows percentage of TEs in the genome; *y* axis indicates specific TE families at a given divergence from the consensus sequence. Distances from consensus of TE subclasses with percentages larger than 1% were plotted. *Rha. kio* = *Rhacophorus kio*; *Rha. dugritei* = *Rhacophorus dugritei*; *Ran. catesbeiana* = *Rana catesbeiana*; *N. parkeri* = *Nanorana parkeri*; *Rhi. marina* = *Rhinella marina*; *X. laevis* = *Xenopus laevis*; *X. tropicalis* = *Xenopus tropicalis*.

Wu et al.
Genomic adaptations for arboreal locomotion in Asian flying treefrogs

PNAS | 3 of 10
https://doi.org/10.1073/pnas.2116342119

DNA/TcMar-Tc1 transposons were the most abundant type among several species of neobatrachians (*R. kio*, *R. dugritei*, *Nanorana parkeri*, and *Rana catesbeiana*) and accounted for a high proportion in *Rhinella marina* but were relatively rare (i.e., ranked below the top five) in mesobatrachian species such as *Xenopus tropicalis* and *Xenopus laevis*. In addition, these anuran genomes contained abundant LTR/gypsy transposons (*SI Appendix*, Table S8), which may have originated from their common ancestor. In total, we obtained 32,093 and 41,291 predicted genes for *R. kio* and *R. dugritei*, respectively, and 87.5% of genes in *R. kio* and 86.4% of genes in *R. dugritei* were annotated in public databases (*SI Appendix*, Table S9). The rough distribution patterns of coding sequence (CDS) length, intron length, and number of CDS transcripts, but not transcript length, were similar in both treefrogs and their close relatives (*SI Appendix*, Fig. S2).

We used chromosomal synteny analysis to determine the structural evolution patterns in the genomes of *R. kio*, *Pyxicephalus adspersus*, *X. laevis*, and *X. tropicalis* and identified 54 ancestor synteny blocks (Fig. 3*A* and *SI Appendix*, Fig. S3) with extensive chromosomal synteny (Fig. 3*B*). Most blocks were located on homologous chromosomes in the different species (Fig. 3 *A* and *B*), although *R. kio* and *P. adspersus* had 13 chromosomes, *X. tropicalis* had 10 chromosomes, and *X. laevis* had 9 chromosomes. Syntenic blocks on Chr 4, Chr 7, and Chr 8 in *X. tropicalis* were distributed on Chr 7 + 10, Chr 9 + 11, and Chr 8 + 13 in *R. kio*, respectively. Chromosome 9 in *R. kio* showed high homology with segments of Chr 3, Chr 7, and Chr 9 in *X. tropicalis* (Fig. 3*B*). Thus, a minimum of one chromosomal fusion and three chromosomal fissions were required for *R. kio* to attain its 13-chromosome structure.

Accelerated Evolution of Limb Development Genes. To identify potential protein-coding genes that evolved significantly faster than average or experienced positive selection, the gene families of the two treefrog species, as well *X. tropicalis*, *X. laevis*, *N. parkeri*, *R. marina*, *Homo sapiens*, *Gallus gallus*, and *Anolis carolinensis*, were retrieved from the reciprocal best hit (RBH)
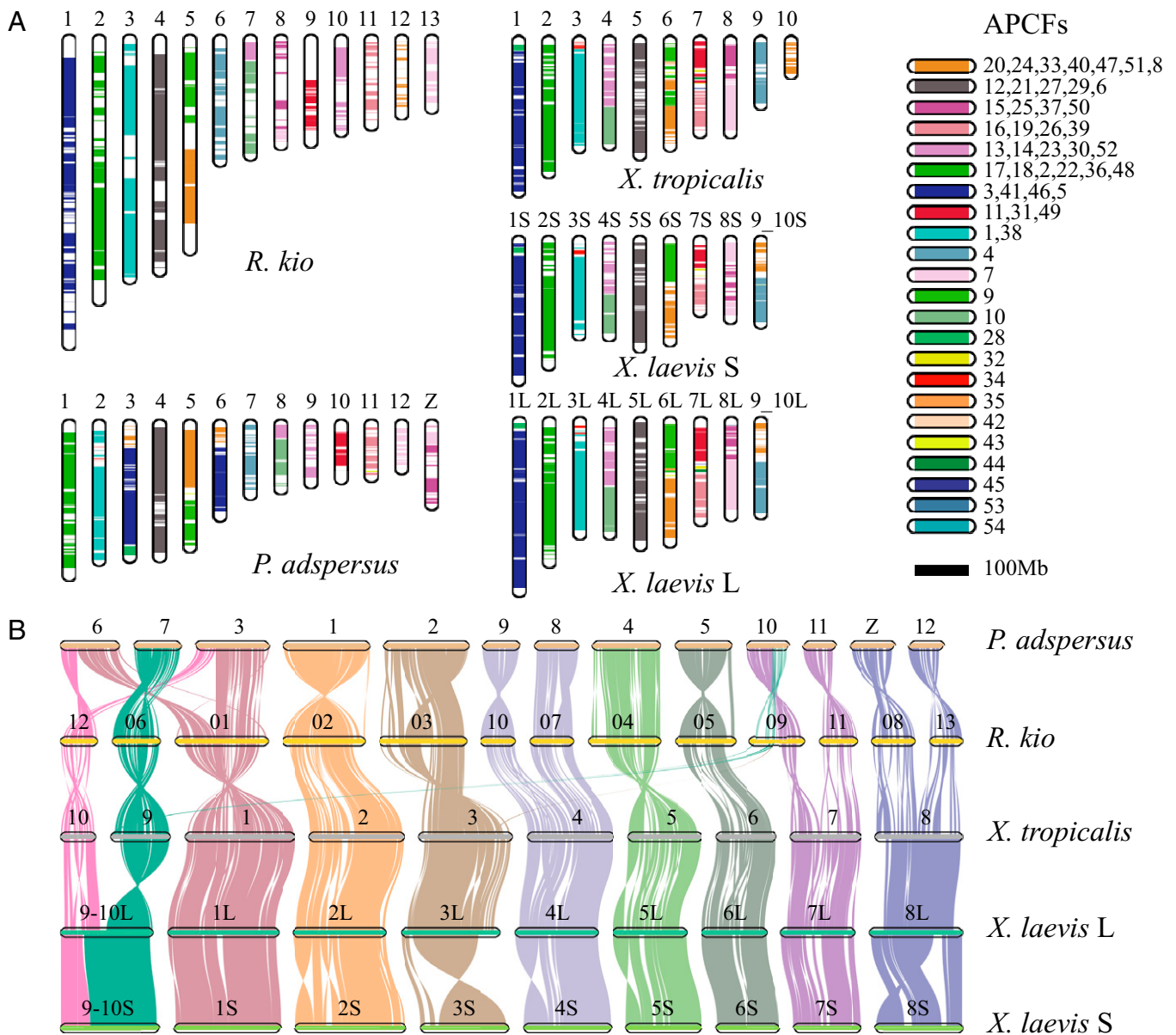

Fig. 3. Chromosome synteny analysis. (*A*) Chromosome synteny analysis: 54 ancestral synteny blocks reconstructed from genomes of *R. kio*, *P. adspersus*, *X. laevis*, and *X. tropicalis*. APCFs, ancestral predicted chromosome fragments. (*B*) Macrosyntenic diagram of chromosome synteny.

results. We identified 455 rapidly evolving genes (REGs) in the treefrogs (*SI Appendix*, Table S10), some of which participate in limb development (Fig. 4*A*). For example, *FGFR2*, which is expressed in the limb ectoderm, apical ectodermal ridge, skeletal anlagen, perichondrium, and periosteum, is necessary for limb formation, with loss of isoform *FGFR2 IIIc* or gain-of-function mutations in *FGFR2* resulting in shortened limbs and digits (17, 18). Furthermore, *FBN2* knockout mice have shorter limb bones than wild-type mice (19). Mutations in *C2D2A*, *ZAK*, *DLX5*, *SF3B4*, and BBS gene families (*BBS2*, *BBS4*, and *BBS7*) are implicated in limb abnormalities (20–24). Therefore, the above REGs are pivotal in limb morphogenesis, especially limb skeletal development. Accelerated evolution of limb-related genes is considered to be correlated with limb morphogenesis adaptation (25). Skeletal system adaptations are related to survival and success in different environments, with the limb bones of arboreal species adapted to cope with the challenges of life in trees. In treefrogs, skeletal adaptations include elongated forelimbs or hands, increased wrist mobility, bony knobs, and bifurcated Y-shaped phalanges (4, 5, 8). Genes related to limb and phalanx morphogenesis display accelerated evolution in the treefrogs, suggesting they may be involved in the evolution of the treefrog skeletal system to help in climbing and grasping.

Genetic Basis for Adhesive Toe Pads. Forty strongly positively selected genes (PSGs, corrected P value < 0.01) were identified in the most recent common ancestor of the studied treefrogs (*Materials and Methods* and *SI Appendix*, Table S11), including the amino acid replacement of T845L in periplakin (PPL) (Fig. 4*B*). This site was highly conserved in mammals, birds, and reptiles (*SI Appendix*, Fig. S4). Functional prediction classified the replacement as intolerant, suggesting that it likely resulted in subtle changes in function (*SI Appendix*, Table S12). The PPL protein is a precursor of the epidermal cornified envelope, which may link the cornified envelope to desmosomes and intermediate filaments. It is also involved in the reorganization of the keratin cytoskeleton network during epidermal keratinocyte differentiation (26, 27). The replacement in PPL was located in a spectrin repeat domain (Fig. 4*B*) and may serve a structural purpose by coordination of cytoskeletal interactions (28). The cytoskeleton creates a dense array of nanoscale peg-like protrusions upon the toe-pad epithelial cells, which are likely essential for mucus drainage and capillary forces (9, 11, 29). Furthermore, *PPL* can control the length of microridges, a type of protrusion on cells covered by mucus, thus contributing to mucus retention by recruiting and binding with keratin cytoskeletal filaments (29). The toe pads of arboreal frogs are covered with mucus, which enables wet adhesion, provides skin lubrication, and limits abrasive wear (9). In addition, the strength and elasticity of these toe pads depend on polygon-arranged cells with nanoscale projections, which may be densely packed with cytoskeletal proteins (30). Thus, *PPL* likely plays a fundamental role in the formation and maintenance of toe-pad epithelial cells in *Rhacophorus* species via interactions with keratin proteins.

Alpha keratins are critical for toe-pad formation (31). In *R. kio* and *R. dugritei*, a total of 48 type I and 23 type II alpha-keratin genes were identified (*SI Appendix*, Table S13). Unlike the expansion of beta keratins in geckos to form climbing bristles (32), the alpha keratins in the treefrogs did not undergo significant expansion (Fig. 4*C* and *SI Appendix*, *SI Text* and Tables S14–S16). We determined the phylogenetic relationships of two types of alpha keratins across vertebrates (Fig. 4*D* and *SI Appendix*, Fig. S5) referring to a previous study (33). Results showed that alpha-keratin gene 45, a *TPK5* homolog, was highly expressed in the toe pads of *R. kio* (Fig. 4 *D* and *E* and *SI Appendix*, Table S17). The type I keratin gene *TPK5* is specifically expressed in the toe pads of *Hyla cinerea* (30). Hylidae (which contains *H. cinerea*) represents an independent lineage

of arboreal frog (30), thus indicating that frogs tend to utilize similar keratins in their toe pads. However, the most phylogenetically close alpha keratin to *TPK5* in *R. kio* is alpha-keratin gene 43, which is not expressed in the toe pads. The similarities and differences among the treefrog clades suggest that a common mechanism exists for the formation of toe pads, which may also explain the limited variation in structure (11). Expansion into new habitats can involve fundamental changes in the integument, which can involve duplications and functional shifts of alpha-keratin genes (34). As an intermediate filament molecule in tetrapods, keratin is essential for integument rigidity. Keratin can maintain its own structural backbone and the cross-linked protein network, even when cells die, and is therefore critical for toe-pad formation (30, 34). The above results suggest that treefrog genes related to the keratin cytoskeleton are involved in the evolution of adhesive toe-pad systems, which are essential for arboreal climbing and fall prevention by providing wet adhesion and cushioning forces (based on its strength).

Developmental Patterns of Webbed Feet. As developmental patterns drive webbed or unwebbed amphibian feet (35) and likely involve differential gene expression regulatory networks, we constructed time-series transcriptome profiles for the hind feet of *R. kio* and *R. dugritei*. Developmental periods followed Gosner (36). Differentiation of the five hind-foot toes as well as the interdigital region where webbing develops occurred from stages 31 to 35 (Fig. 5*A*). From stages 35 to 39, the interdigital area in *R. kio* was enlarged and connected with skin tissue, whereas interdigital area expansion in *R. dugritei* was indistinct. Webbing was measured during development based on "sinuosity," a dimensionless ratio that measures the extent of webbing on the feet (35). Results showed that *R. kio* had more webbing (i.e., lower sinuosity, P < 0.01) than *R. dugritei* after stage 37 (*SI Appendix*, Table S18), indicating a key period for the emergence of webbing. Sinuosity trends distinguished two developmental patterns (Fig. 5*B*). In unwebbed *R. dugritei*, sinuosity increased from the juvenile to adult stage, showing similar patterns as unwebbed salamanders, where shape changes via outgrowths of toe tips or via differential growth of skin tissue between digits (35). In contrast, the degree of webbing in webbed *R. kio* exhibits slight differences compared to webbed salamanders, whose webbed feet result from the retention of a juvenile morphology (i.e., invariant sinuosity) (35). Divergent developmental patterns were also shown based on the time-ordered transcriptomes (*SI Appendix*, Fig. S6).

We used time-ordered gene coexpression network (TO-GCN) analysis (37) to visualize data on gene expression, timing, and conditions. Genes positively coexpressed in *R. kio* only (termed Rkio+Rdug0) were considered likely to be involved in the formation and development of webbing. Based on TO-GCN analysis, 410 transcription factor (TF) genes were assigned into 18 time-ordered levels (*SI Appendix*, Fig. S7). The TF expression in the time-ordered levels roughly matched limb development in *R. kio*, as indicated by the relatively high expression levels along the diagonal in Fig. 5*C* and *SI Appendix*, Fig. S8. The high expression of these genes suggested involvement in consecutive developmental periods. Enrichment analyses identified the function of genes at each level, and the development-related categories overrepresented at multiple levels were further explored (*SI Appendix*, Table S19).

The Wnt signaling-related pathways, which are implicated in the patterning and outgrowth of vertebrate limbs as well as bone phenotypes (38), were overrepresented in the first four levels, which correspond to the five-toes differentiation period (stages 31 to 35). A subnetwork of all Wnt signaling-related genes in Rkio+Rdug0 identified *TCF7L1* and *TCF7L2* as potential hub effector molecules (Fig. 5*D*). As downstream
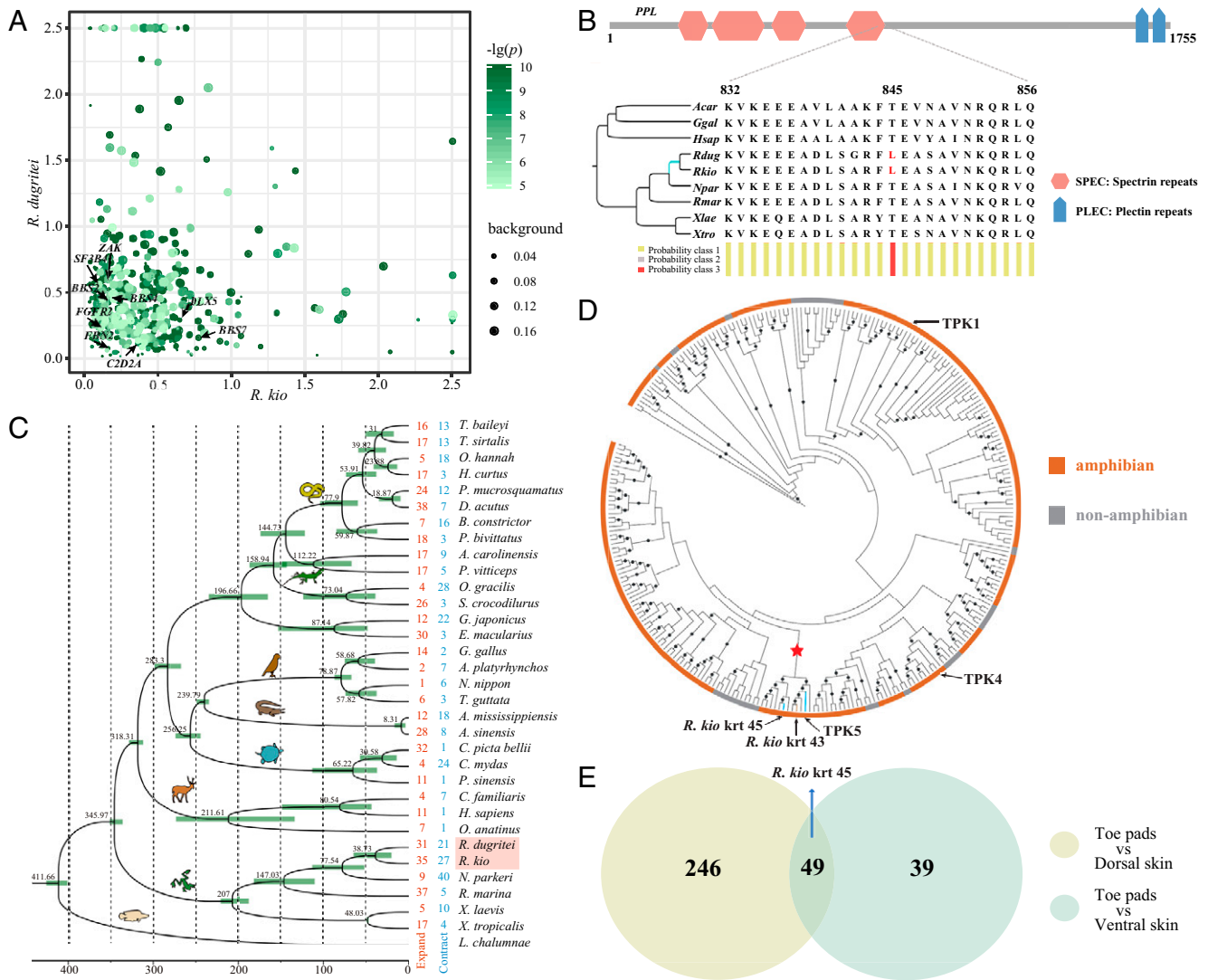
Wu et al.
Genomic adaptations for arboreal locomotion in Asian flying treefrogs

PNAS | 5 of 10
https://doi.org/10.1073/pnas.2116342119

EVOLUTION

Fig. 4. Analysis of gene families in treefrogs. (*A*) Rapidly evolving protein-coding genes (REGs). Darkness of color represents significance. Size of dots is the omega (ω) value of background genes. *x* axis and *y* axis represent ω values of genes in *R. kio* and *R. dugritei*, respectively. Dots labeled are genes involved in limb development. (*B*) Shared amino acid replacements of *PPL* in *Rhacophorus*. Lower bars indicate posterior probabilities for three site-classes as calculated using CODEML in PAML. Class 1 sites are evolving under purifying selection (very low rate of nonsynonymous compared with synonymous substitutions), class 2 under neutral selection (similar rate of nonsynonymous and synonymous substitutions), and class 3 sites under positive selection (high rate of nonsynonymous compared with synonymous substitutions). (*C*) Phylogenetic position of *Rhacophorus* members relative to other vertebrates. Estimated divergence times were scaled to branch lengths of phylogenetic tree. Green bars represent 95% credibility intervals of the estimated posterior distributions of divergence times. Bayesian posterior probabilities are 1.0 for all nodes. Numbers in orange and blue represent expanded and contracted gene families, respectively. (*D*) Phylogenetic relationships of type I alpha-keratin genes across vertebrates. Each branch is a keratin gene. Orange branches are anurans keratins; gray branches are *H. sapiens* or *A. carolinensis* keratins. Red asterisk denotes anuran-specific branch, including TPK5 and *R. kio* toe-pad-specific keratins. Dots on branches represent bootstrap values >75. (*E*) Venn diagram of highly expressed genes in toe pads compared with dorsal and ventral skin.

transcriptional activators or repressors, *TCF7L1* and *TCF7L2* are essential for postaxial digit formation, osteogenesis, and limb morphogenesis (39, 40). Thus, differential gene expression patterns were found between the strongly and weakly webbed feet before webbing formation, although the sinuosity values were similar (at stage 35). Wnt signaling may mediate the differences in feet morphologies (i.e., webbed or unwebbed) among treefrogs via regulation of limb development. Based on Gene Ontology (GO) enrichment, terms related to skeletal system development, ossification, and neuron differentiation were overrepresented by genes in Rkio+Rdug0 (*SI Appendix*, Table S19), suggesting that genes involved in limb development can regulate degree of webbing in amphibians, consistent with morphological comparisons in salamanders (35).

At levels 7 to 12, genes were enriched in vascular remodeling-related terms (*SI Appendix*, Table S19). These genes were relatively highly expressed from stages 35 to 39 (*SI Appendix*, Fig. S9) in *R. kio*, which coincided with the appearance of vascular remodeling in the interdigital tissue of *X. laevis* (41), implying that development of interdigital webbing in anurans may be blood-vessel-dependent. The cardiovascular system supplies essential oxygen, nutrients, and molecular signals during embryonic development (42). The subnetwork of blood-vessel-remodeling-related genes identified *Hes5* and *Ednrb* as potential hub genes (Fig. 5*E*). *Hes5* regulates vascular remodeling and is an essential effector for Notch signaling, which regulates the proliferation and differentiation of cells (43). Located primarily in vascular endothelial cells, *Ednrb* is a major
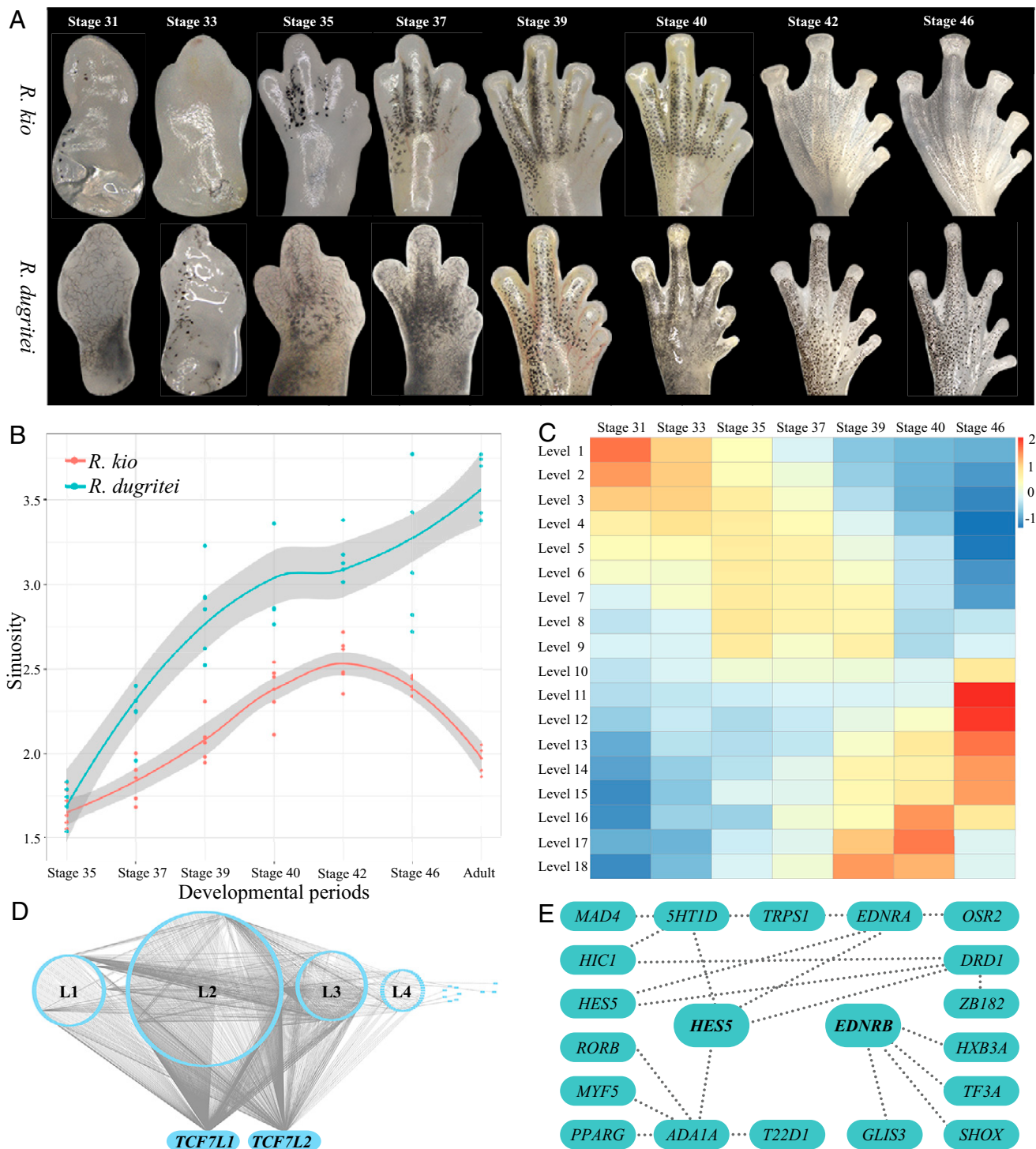
Fig. 5. TO-GCN of tadpole feet of *R. kio* and *R. dugritei*. (*A*) Morphological changes during the development of feet (stages 31 to 46) in tadpoles. (*B*) Sinuosity as measured over the developmental processes of both treefrogs. Larger sinuosity indicates a smaller extent of webbing. (*C*) Heat map at each time point of TF genes at each level of TO-GCN Rkio+Rdug0 in *R. kio*. The upper quartile TPM values were normalized to z-scores first, and the z-scores of all TFs at each level were then averaged. (*D*) Subnetwork of genes involved in Wnt signaling-related pathways. *TCF7L1* and *TCF7L2* were hub genes. (*E*) Subnetwork of genes enriched in vasculature-related terms. *Hes5* and *Ednrb* were hub genes.

regulator of vascular function, including vasoconstriction, vaso-dilation, and cell proliferation (44). Amphibians form webbed digits through the proliferation of the interdigital regions (45). Therefore, genes associated with vasculature may promote interdigital area growth by the proliferation of capillaries to carry nutrients and signals.

Increases in vascular density in the *Xenopus* palm can promote the accumulation of reactive oxygen species (ROS), which may induce interdigital cell death (ICD) (41, 42) and hinder webbing formation. Programmed ICD determines the formation of free or webbed digits in many amniotes (45). Inhibition of ICD-related pathways in species with free digits can result in

Wu et al.
Genomic adaptations for arboreal locomotion in Asian flying treefrogs

PNAS | 7 of 10
https://doi.org/10.1073/pnas.2116342119

syndactyly (46). However, ICD is not reported in amphibians (45), except in a few salamander species (47), suggesting that webbed frogs can control the concentration of ROS in the interdigital regions to avoid ICD. Aquatic larvae are ecologically isolated from oxygen-rich air, which may help in the development of amphibian limbs without ICD (41). Here, *SESN2* and *SESN3*, which encode antioxidant modulators of peroxiredoxins and can regulate ROS levels (48), were enriched in ROS-related terms (*SI Appendix*, Table S19). In mice, decreased antioxidant enzyme activity in the interdigital regions causes an increase in ROS levels, which can accelerate the ICD process (49). Therefore, in addition to environmental factors, antioxidant genes, such as *SESN2* and *SESN3*, may provide another layer of protection during webbing formation in gliding treefrogs via regulation of ROS accumulation and cell apoptosis avoidance.

Overall, our results revealed marked differences in the developmental patterns of webbed and unwebbed toes, and webbed traits may be shaped by specific expression patterns of Wnt signaling-related and angiogenesis-related genes involved in limb development and vascular remodeling. Of note, we only evaluated and sequenced the hind limb because of its earlier development, larger size, accessibility, and ease of measurement. Pedal webbing in "flying" treefrogs may be a functional expansion, given its initial use in swimming, and manus webbing may be more important for exploiting the vertical niche. Thus, further studies are needed to verify the similarity in expression patterns between hands and feet. In addition, as webbing in anurans is a continuous variable serving multiple functions, additional research across a wider range of amphibian species is needed.

Conclusions

Genetic adaptation to new niches and variation in complex traits are key factors in speciation and diversification. Here, we explored the genetic basis for complex traits in treefrogs that facilitate climbing and gliding to provide a foundation for understanding the adaptive strategies of amphibians to vertical niches. Genomic analysis revealed that skeletal- and cytoskeletal-related genes played key roles in the evolution of treefrog climbing and grasping systems. We also identified a key coexpression network involved in the formation of webbed feet. Overall, our results showed the importance of local adaptation in shaping phenotypes and locomotion patterns.

Materials and Methods

Genome Sequencing, Assembly, and Annotation. Female specimens of *R. kio* (sample ID: CIB118517) and *R. dugritei* (ID: CIB118518) were collected from Xishuangbanna, Yunnan, and Ya'an, Sichuan, China, respectively. Vouchers were stored in the Herpetological Museum of the Chengdu Institute of Biology, Chinese Academy of Sciences. Genomic DNA was extracted from muscle using QIAGEN Genomic DNA Extraction Kit (Qiagen). For sequencing the genome of *R. kio*, we generated 543.49 Gb (~204× coverage) of clean paired-end reads via the Illumina NovaSeq 6000 platform following the manufacturer's standard protocol and 143.47 Gb of subreads (~54× coverage) via a PacBio Sequel instrument. Genome size of *R. kio* was evaluated via the k-mer algorithm (k = 17; *SI Appendix*, Fig. S10). Sequencing of the *R. dugritei* genome using similar strategies generated 132.51 Gb of clean reads via the 10× Genomics Chromium platform and 60.98 Gb of subreads via the PacBio Sequel platform. The prepared Hi-C library for *R. kio* was used for paired-end sequencing with the Illumina NovaSeq 6000 platform. Additionally, Illumina sequencing data (paired-end, 150 bp) were generated for several other species of *Rhacophorus*. All whole-genome sequencing and resequencing data used in this study are listed in *SI Appendix*, Tables S20–S22. Hybrid assembly strategies were adopted for de novo assembly. Gene structures were determined by combing ab initio methods and homology-based annotation. Gene functions were annotated via aligning the integrated gene set against public databases. The detailed information of assembly, annotation, and chromosome synteny analysis are recorded in *SI Appendix, SI Text*.

Gene-Family Analysis. Protein sequences from the genomes of 33 vertebrate species were used to reconstruct the phylogenetic tree (*SI Appendix, SI Text*).

We removed the low-quality hits (identity <30%; coverage <30%) based on the self-to-self alignments conducted for protein sequences from species with available genomes using BLASTP v2.7.1 (E-value = 1e-5) (50). Then, orthologous groups were constructed using ORTHOMCL v2.0.9 (51) with the default settings based on the filtered BLASTP results. Genes from one species that did not cluster into a gene family were considered species-specific. We employed CAFÉ 3.1 (52) to analyze expansion and contraction of gene families. When the copy number of focused branch-lineages was higher or lower than its ancestral branch lineage, the gene family was regarded as significantly expanded or contracted, respectively (Viterbi $P \leq 0.05$). Significantly overrepresented GO terms among these significantly expanded gene families were identified using topGO v2.38.1 ($P \leq 0.01$) (53). False discovery rate (FDR) with Benjamini–Hochberg procedure was used for multiple testing correction.

Identification of REGs and PSGs. To identify potential PSGs, gene families of *R. kio*, *R. dugritei*, *H. sapiens*, *G. gallus*, *A. carolinensis*, *N. parkeri*, *R. marina*, *X. laevis*, and *X. tropicalis* were retrieved from the RBH results as described above. Then, we extracted the single gene families and aligned the protein sequences from each family using MUSCLE v3.8.31 (54) with the default parameters. Next, corresponding CDS alignments were back-translated using PAL2NAL v14 (55), and the conserved CDS alignments were extracted by Gblocks v0.91b (56) and used for further identification of REGs and PSGs.

The branch model of CODEML in PAML v4.7 (57) was used to test for potential REGs, by setting *R kio* and *R. dugritei* as the foreground branch and the others as background branches. The null hypothesis was that the omega (ω) value of each branch was equal; the alternative hypothesis was that the ω value on the foreground branch was not equal to those on the background branches. Then, a likelihood ratio test (LRT) was performed after correcting P values using the FDR test with Bonferroni correction. Identified genes were considered REGs when the ω value on the foreground branch was greater than that on the background branches (regardless of whether it is greater than 1), and the corrected P value < 0.05.

The branch-site model of CODEML in PAML v4.7 was used to identify potential PSGs with *R. kio*, *R. dugritei*, and *R. kio+R. dugritei* set as foreground branches and the others as background branches. The null hypothesis was that the ω value of each site on each foreground branch was ≤ 1, and the alternative hypothesis was ω values were > 1. LRT was performed setting the null distribution to a 50:50 mixture of χ^2 distributions with 1 degree of freedom and a point mass of zero. FDR testing with Bonferroni correction was used for multiple testing correction. PSGs had a corrected P < 0.01 and contained at least one positively selected site with a posterior probability greater than 0.95 based on Bayes Empirical Bayes analysis. PROVEAN (Protein Variation Effect Analyzer) analyses were performed for functional prediction (58). The default threshold of the PROVEAN score is 2.5; when the PROVEAN score is larger than 2.5, it is classified as neutral; when the PROVEAN score is smaller than 2.5, it is classified as deleterious.

Alpha-Keratin Gene Analyses. Our pipeline of alpha-keratin gene analyses followed research for *Leptobrachium leishanense* (33). The detailed information is recorded in *SI Appendix, SI Text*. Transcriptome analysis of toe-specific alpha-keratin was performed as follows. Because adhesion of toe pads mainly depends on the epidermal structure, we sequenced transcriptomes of toe pads, dorsal skin, and ventral skin from three adult *R. kio* to identify pad-specific expressed genes. RNAs were extracted based on the protocols (*SI Appendix, SI Text*) and then paired-end-sequenced on an Illumina NovaSeq 6000 instrument. After quality control (QC), we mapped the clean reads to the genome of *R. kio* using Hisat2 v2.1.0 (59). Counts of each sample were calculated using featureCounts in the Rsubread package (60), and differential expression analysis used DESeq2 v1.30.0 (61). Toe-pad-specific genes were required to have an absolute value of log 2-fold change ≥ 1, and corrected P < 0.05; we focused mainly on the alpha-keratins.

Gliding Experiments. *R. kio* and *R. dugritei* were used to explore the effect of foot webbing on gliding. We assessed the relative areas of webbed interdigital tissues of 10 adult males of each species in comparison to their overall interdigital areas. Morphological measurement used a square grid method and significance of differences was calculated by Student's t test. A grid wall of 10- × 10-cm cells was used to determine angle of descent. Both species were allowed to jump from heights of 1.0, 1.5, and 2.0 m, which was documented using a GoPro HERO 5 camera. In the gliding experiment, two attempts were made by each individual with a 24-h resting period between each attempt. A sponge was placed on the ground to prevent the treefrogs from being injured. Analysis of the videos detected the horizontal angle and ground clearance of each test. All procedures were conducted in accordance with the approval of the Animal Experiment Ethics Committee of the

Chengdu Institution of Biology, Chinese Academy of Sciences. Experiments using higher heights were not pursued owing to concerns for the animals' welfare.

Determining the Developmental Stages of Tadpole Limbs and Measuring Webbing. Developmental periods of tadpoles were divided according to Gosner (36). We explored morphological changes during feet development in tadpoles, especially from stages 31 to 46, which defined three major stages: 1) five fingers (stages 31 to 35), 2) five-finger growth (stages 37 to 40) and interdigital tissue connection or loss, and 3) preparation for landing (stages 42 to 46), including emergence of forelimbs and gradual development of the limbs. We measured sinuosity—a dimensionless ratio that allows discrimination of different foot morphologies and determines the amount of webbing (higher sinuosity suggests less webbing, and vice versa) (35)—to define the degree of webbing during development. This was calculated by the length of the outline of the foot from the tip of digit one to digit five divided by the width of the foot (diameter or width of the foot, from the tip of digit one to the tip of digit five) (35). We photographed the feet using a camera (Leica DFC450 C; Leica Microsystems Ltd.) and constructed a montage of multifocal photographs using Helicon Focus (7.0.2 Pro). Sinuosity was measured using Image J2 (https://github.com/imagej/imagej2).

Time-Series Transcriptome Analysis of Webbed and Unwebbed Feet. We tested the hypothesis that webbing morphology was related to differences in gene expression during limb development. Time-ordered gene expression analysis of limb development from the formation of the paddle-like foot to completion was employed. The hind limb was evaluated because of its earlier development, larger size, accessibility, and ease of measurement; forelimb emergence did not start until stage 42, near the completion of metamorphosis. We sampled the critical period of webbing growth for the hindlimb (stage 37), as well as the periods immediately before and after. The sample information is listed in *SI Appendix*, Table S23. Because the very small feet of tadpoles barely meet the tissue needs for sequencing, we used a mixed sample strategy, with no fewer than three individuals (3 to 5) per sample. RNA extraction, library preparation, and sequencing were done as detailed above. After QC, we mapped the clean reads to their own reference genomes using Hisat2 v2.1.0 and quantified expression with Stringtie v2.0.3 (59). We then extracted the expressional matrix of transcript per million (TPM) according to their orthologous gene set to construct a TO-GCN (37) (*SI Appendix, SI Text*).

Data Availability. Raw sequencing data and genome assembly were deposited in the China National GeneBank Nucleotide Sequence Archive with accession number CNP0002375. All other data are included in the article and/or supporting information.

1. M. Taverne *et al.*, Convergence in the functional properties of forelimb muscles in carnivorans: Adaptations to an arboreal lifestyle? *Biol. J. Linn. Soc. Lond.* **125**, 250–263 (2018).
2. G. Byrnes, A. J. Spence, Ecological and biomechanical insights into the evolution of gliding in mammals. *Integr. Comp. Biol.* **51**, 991–1001 (2011).
3. M. Cartmill, "Climbing" in *Functional Vertebrate Morphology*, M. Hildebrand, D. M. Bramble, K. F. Liem, D. B. Wake, Eds. (Harvard University Press, 1985), pp. 73–88.
4. A. S. Manzano, V. Abdala, A. Herrel, Morphology and function of the forelimb in arboreal frogs: Specializations for grasping ability? *J. Anat.* **213**, 296–307 (2008).
5. N. X. Dang *et al.*, The specialisation of the third metacarpal and hand in arboreal frogs: Adaptation for arboreal habitat? *Acta Zool.* **99**, 115–125 (2018).
6. Y. J. Feng *et al.*, Phylogenomics reveals rapid, simultaneous diversification of three major clades of Gondwanan frogs at the Cretaceous-Paleogene boundary. *Proc. Natl. Acad. Sci. U.S.A.* **114**, E5864–E5870 (2017).
7. W. J. P. Barnes, P. J. P. Goodwyn, M. Nokhbatolfoghahai, S. N. Gorb, Elastic modulus of tree frog adhesive toe pads. *J. Comp. Physiol. A Neuroethol. Sens. Neural Behav. Physiol.* **197**, 969–978 (2011).
8. L. A. Gray, J. C. O'Reilly, K. C. Nishikawa, Evolution of forelimb movement patterns for prey manipulation in anurans. *J. Exp. Zool.* **277**, 417–424 (1997).
9. W. Federle, W. J. P. Barnes, W. Baumgartner, P. Drechsler, J. M. Smith, Wet but not slippery: Boundary friction in tree frog adhesive toe pads. *J. R. Soc. Interface* **3**, 689–697 (2006).
10. K. Autumn *et al.*, Evidence for van der Waals adhesion in gecko setae. *Proc. Natl. Acad. Sci. U.S.A.* **99**, 12252–12256 (2002).
11. W. J. P. Barnes, Functional morphology and design constraints of smooth adhesive pads. *MRS Bull.* **32**, 479–485 (2007).
12. J. A. Oliver, "Gliding" in amphibians and reptiles, with a remark on an arboreal adaptation in the lizard, *Anolis carolinensis carolinensis* Voigt. *Am. Nat.* **85**, 171–176 (1951).
13. J. Dong, Y. Deng, J. Liu, Treefrogs near the top of a tropical rainforest. *Front. Ecol. Environ.* **19**, 460 (2021).
14. S. B. Emerson, M. A. R. Koehl, The interaction of behavioral and morphological change in the evolution of a novel locomotor type: "flying" frogs. *Evolution* **44**, 1931–1946 (1990).
15. M. Kuramoto, A comparative study of karyotypes in the treefrogs (Family Rhacophoridae) from Japan and Taiwan. *Caryologia* **30**, 333–342 (1977).
16. M. Seppey, M. Manni, E. M. Zdobnov, BUSCO: Assessing genome assembly and annotation completeness. *Methods Mol. Biol.* **1962**, 227–245 (2019).
17. J. E. Salva, R. R. Roberts, T. S. Stucky, A. E. Merrill, Nuclear FGFR2 regulates musculoskeletal integration within the developing limb. *Dev. Dyn.* **248**, 233–246 (2019).
18. V. P. Eswarakumar *et al.*, The IIIc alternative of Fgfr2 is a positive regulator of bone formation. *Development* **129**, 3783–3793 (2002).
19. R. Boregowda, E. Paul, J. White, T. M. Ritty, Bone and soft connective tissue alterations result from loss of fibrillin-2 expression. *Matrix Biol.* **27**, 661–666 (2008).
20. J. Tallila, E. Jakkula, L. Peltonen, R. Salonen, M. Kestilä, Identification of CC2D2A as a Meckel syndrome gene adds an important piece to the ciliopathy puzzle. *Am. J. Hum. Genet.* **82**, 1361–1367 (2008).
21. M. Spielmann *et al.*, Exome sequencing and CRISPR/Cas genome editing identify mutations of ZAK as a cause of limb defects in humans and mice. *Genome Res.* **26**, 183–191 (2016).
22. H. E. Shamseldin, M. A. Faden, W. Alashram, F. S. Alkuraya, Identification of a novel DLX5 mutation in a family with autosomal recessive split hand and foot malformation. *J. Med. Genet.* **49**, 16–20 (2012).
23. F. P. Bernier *et al.*; FORGE Canada Consortium, Haploinsufficiency of SF3B4, a component of the pre-mRNA spliceosomal complex, causes Nager syndrome. *Am. J. Hum. Genet.* **90**, 925–933 (2012).
24. C. Deveault *et al.*, BBS genotype-phenotype assessment of a multiethnic patient cohort calls for a revision of the disease definition. *Hum. Mutat.* **32**, 610–619 (2011).
25. M. Tollis *et al.*, Comparative genomics reveals accelerated evolution in conserved pathways during the diversification of anole lizards. *Genome Biol. Evol.* **10**, 489–506 (2018).
26. M. Gujrati, R. Mittal, L. Ekal, R. K. Mishra, SUMOylation of periplakin is critical for efficient reorganization of keratin filament network. *Mol. Biol. Cell* **30**, 357–369 (2019).
27. H. A. Long, V. Boczonadi, L. McInroy, M. Goldberg, A. Määttä, Periplakin-dependent re-organisation of keratin cytoskeleton and loss of collective migration in keratin-8-downregulated epithelial sheets. *J. Cell Sci.* **119**, 5147–5159 (2006).
28. K. Djinovic-Carugo, M. Gautel, J. Ylänne, P. Young, The spectrin repeat: A structural platform for cytoskeletal protein assemblies. *FEBS Lett.* **513**, 119–123 (2002).
29. Y. Inaba, V. Chauhan, A. P. van Loon, L. S. Choudhury, A. Sagasti, Keratins and the plakin family cytolinker proteins control the length of epithelial microridge protrusions. *eLife* **9**, 1–27 (2020).
30. W. Vandebergh, M. Maex, F. Bossuyt, I. Van Bocxlaer, Recurrent functional divergence of early tetrapod keratins in amphibian toe pads and mammalian hair. *Biol. Lett.* **9**, 20130051 (2013).
31. S. Chakraborti, T. C. Nag, D. Das, T. Sanyal Chatterjee, S. K. De, Cytokeratin localization in toe pads of the anuran amphibian *Philautus annandalii* (Boulenger, 1906). *Tissue Cell* **46**, 165–169 (2014).
32. Y. Liu *et al.*, Gekko japonicus genome reveals evolution of adhesive toe pads and tail regeneration. *Nat Commun* **6**, 1–11 (2015).
33. J. Li *et al.*, Genomic and transcriptomic insights into molecular basis of sexually dimorphic nuptial spines in *Leptobrachium leishanense*. *Nat. Commun.* **10**, 5551 (2019).
34. W. Vandebergh, F. Bossuyt, Radiation and functional diversification of alpha keratins during early vertebrate evolution. *Mol. Biol. Evol.* **29**, 995–1004 (2012).
35. M. Jaekel, D. B. Wake, Developmental processes underlying the evolution of a derived foot morphology in salamanders. *Proc. Natl. Acad. Sci. U.S.A.* **104**, 20437–20442 (2007).
36. K. Gosner, A simplified table for staging anuran embryos and larvae with notes on identification. *Herpetologica* **16**, 183–190 (1960).
37. Y. M. Chang *et al.*, Comparative transcriptomics method to infer gene coexpression networks and its applications to maize and rice leaf transcriptomes. *Proc. Natl. Acad. Sci. U.S.A.* **116**, 3091–3099 (2019).
38. P. Geetha-Loganathan, S. Nimmagadda, M. Scaal, Wnt signaling in limb organogenesis. *Organogenesis* **4**, 109–115 (2008).
39. Z. Li *et al.*, Role of TCF/LEF transcription factors in bone development and osteogenesis. *Int. J. Med. Sci.* **15**, 1415–1422 (2018).
40. C. I. Wu *et al.*, Function of Wnt/β-catenin in counteracting Tcf3 repression through the Tcf3-β-catenin interaction. *Development* **139**, 2118–2129 (2012).
41. I. R. Cordeiro *et al.*, Environmental oxygen exposure allows for the evolution of interdigital cell death in limb patterning. *Dev. Cell* **50**, 155–166.e4 (2019).

EVOLUTION

Wu et al.
Genomic adaptations for arboreal locomotion in Asian flying treefrogs

PNAS | 9 of 10
https://doi.org/10.1073/pnas.2116342119

42. I. Eshkar-Oren, S. Krief, N. Ferrara, A. M. Elliott, E. Zelzer, Vascular patterning regulates interdigital cell death by a ROS-mediated mechanism. *Development* **142**, 672–680 (2015).

43. M. Kitagawa *et al.*, Hes1 and Hes5 regulate vascular remodeling and arterial specification of endothelial cells in brain vascular development. *Mech. Dev.* **130**, 458–466 (2013).

44. M. Q. Mazzuca, R. A. Khalil, Vascular endothelin receptor type B: Structure, function and dysregulation in vascular disease. *Biochem. Pharmacol.* **84**, 147–162 (2012).

45. J. A. Cameron, J. F. Fallon, The absence of cell death during development of free digits in amphibians. *Dev. Biol.* **55**, 331–338 (1977).

46. C. I. Lorda-Diez, J. A. Montero, J. A. Garcia-Porrero, J. M. Hurle, Interdigital tissue regression in the developing limb of vertebrates. *Int. J. Dev. Biol.* **59**, 55–62 (2015).

47. R. A. Franssen, S. Marks, D. Wake, N. Shubin, Limb chondrogenesis of the seepage salamander, *Desmognathus aeneus* (Amphibia: Plethodontidae). *J. Morphol.* **265**, 87–101 (2005).

48. P. B. Kopnin, L. S. Agapova, B. P. Kopnin, P. M. Chumakov, Repression of sestrin family genes contributes to oncogenic Ras-induced reactive oxygen species up-regulation and genetic instability. *Cancer Res.* **67**, 4671–4678 (2007).

49. D. Schnabel *et al.*, Expression and regulation of antioxidant enzymes in the developing limb support a function of ROS in interdigital cell death. *Dev. Biol.* **291**, 291–299 (2006).

50. S. F. Altschul, W. Gish, W. Miller, E. W. Myers, D. J. Lipman, Basic local alignment search tool. *J. Mol. Biol.* **215**, 403–410 (1990).

51. L. Li, C. J. Stoeckert Jr., D. S. Roos, OrthoMCL: Identification of ortholog groups for eukaryotic genomes. *Genome Res.* **13**, 2178–2189 (2003).

52. T. De Bie, N. Cristianini, J. P. Demuth, M. W. Hahn, CAFE: A computational tool for the study of gene family evolution. *Bioinformatics* **22**, 1269–1271 (2006).

53. A. A. Alexa, J. Rahnenfuhrer, M. A. Alexa, topGO: Enrichment Analysis for Gene Ontology. R package version 2.38.1 (2020).

54. R. C. Edgar, MUSCLE: Multiple sequence alignment with high accuracy and high throughput. *Nucleic Acids Res.* **32**, 1792–1797 (2004).

55. M. Suyama, D. Torrents, P. Bork, PAL2NAL: Robust conversion of protein sequence alignments into the corresponding codon alignments. *Nucleic Acids Res.* **34**, W609–W612 (2006).

56. J. Castresana, Selection of conserved blocks from multiple alignments for their use in phylogenetic analysis. *Mol. Biol. Evol.* **17**, 540–552 (2000).

57. Z. Yang, PAML 4: Phylogenetic analysis by maximum likelihood. *Mol. Biol. Evol.* **24**, 1586–1591 (2007).

58. Y. Choi, G. E. Sims, S. Murphy, J. R. Miller, A. P. Chan, Predicting the functional effect of amino acid substitutions and indels. *PLoS One* **7**, e46688 (2012).

59. M. Pertea, D. Kim, G. M. Pertea, J. T. Leek, S. L. Salzberg, Transcript-level expression analysis of RNA-seq experiments with HISAT, StringTie and Ballgown. *Nat. Protoc.* **11**, 1650–1667 (2016).

60. Y. Liao, G. K. Smyth, W. Shi, The R package Rsubread is easier, faster, cheaper and better for alignment and quantification of RNA sequencing reads. *Nucleic Acids Res.* **47**, e47 (2019).

61. M. I. Love, W. Huber, S. Anders, Moderated estimation of fold change and dispersion for RNA-seq data with DESeq2. *Genome Biol.* **15**, 550 (2014).